JTTEE 2:235-242

Application of Fracture Mechanics to the Interpretation of Bond Strength Data from ASTM Standard C633-79

W. Han, E.F. Rybicki, and J.R. Shadley

The debonding specimen used in ASTM Standard C633-79 has a nonuniform stress distribution at the interface between the coating and the substrate.[1] This means that bond strengths determined according to the standard could be significantly lower than actual strengths. A new specimen, 50% longer than the standard specimen, was developed to alleviate this problem. The elongated specimen has a uniform stress distribution that is equal to the uniform stress assumed by ASTM Standard C633-79. Thus, bond strengths obtained using the elongated specimen are higher and more representative of the actual bond strength than estimates obtained from the standard specimen. In this work, a procedure is developed to transform the existing bond strength values obtained using the C633-79 Standard specimens to the more representative bond strength values that would be obtained if the tests were repeated using the elongated specimens. A combination of finite-element analyses and laboratory test data is used to identify the relation between the bond strength values of standard specimens and those of elongated specimens. Examples are presented and the procedure is verified by comparisons with bond strength data for Colmonoy No. 6 and aluminum oxide coatings.

1. Introduction

BOND strength is an important property of thermal spray coatings. It is a measure of the ability of the coating to adhere to the substrate. One widely used bond strength test in United States industry and research is the ASTM Standard C633-79, entitled "Standard Test Method for Adhesion or Cohesive Strength of Flame-Sprayed Coatings."[2-6] According to the ASTM Standard C633-79, tests are performed by first applying the coating to the end of a 25.4 mm (1 in.) long by 25.4 mm (1 in.) diameter cylinder of the substrate metal. The coating surface is bonded to the end of another cylinder of the same material and geometry, as illustrated in Fig. 1. The force to pull the cylinders apart is recorded. The bond strength is the ultimate bond stress calculated by dividing the force to pull the cylinders apart, by the area of the 25.4 mm (1 in.) diameter cylinder. In a successful test, debonding occurs between the coating and the substrate or within the coating.

A key assumption in the procedure is that the stress distribution is uniform over the interface between the coating and the substrate. In a previous work,[1] it was found that the ASTM Standard C633-79 specimen has a nonuniform stress distribution at the interface between the coating and the substrate. Therefore, somewhere on the interface, the stress is higher than the average stress. This means that bond strengths determined according to the standard could be significantly lower than actual strengths.

Key Words: adhesion, ASTM C633-79, bond strength, energy release rate, finite element modeling, fracture mechanics, stress distributions, tensile adhesion test

W. Han, E.F. Rybicki, and **J.R. Shadley,** Mechanical Engineering Department, The University of Tulsa, 600 South College Avenue, Tulsa, OK 74104-3189, USA.

The design for a new, elongated specimen was presented in a previous work.[1] Because of the uniform stress distribution, bond strength estimates obtained using elongated specimens are higher than estimates obtained from standard specimens. There is a sizeable amount of bond strength data obtained using the ASTM C633-79 specimens. Although it would be desirable to redo all of the tests using an elongated specimen, it is expensive and time consuming. Therefore, the goal of this work is to develop a procedure to transform the existing bond strength values

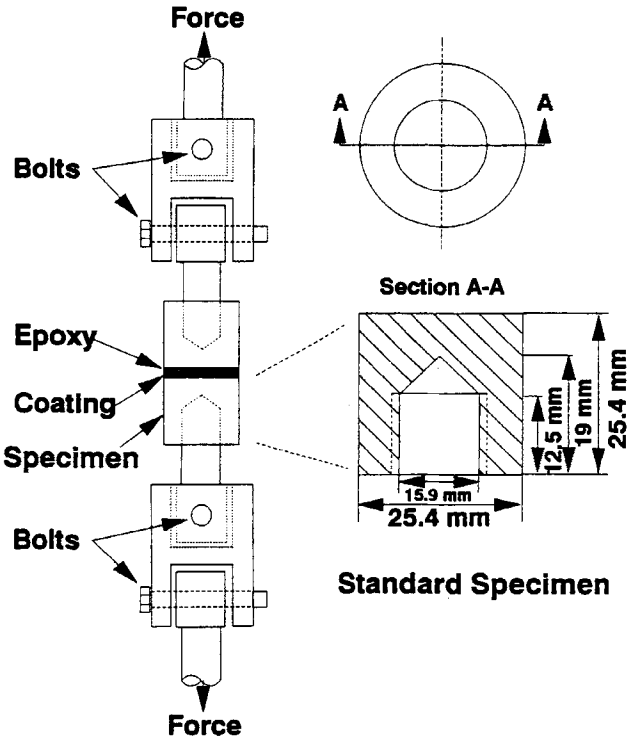

Fig. 1 ASTM C633-79 self-aligning test fixture and specimen.

obtained from the C633-79 Standard specimens to more representative values that would be obtained, if the tests were repeated using the elongated specimens.

2. Approach

The approach to meeting the goal of determining bond strengths of elongated specimens from standard specimen data involves a combination of finite-element analyses and laboratory tests. A key ingredient to the approach is the selection of a fracture criterion to represent debonding of the standard specimen. The same criterion is assumed to hold for the elongated specimen. Based on the fracture criterion and finite-element analyses, a relation between the bond strength of the elongated specimen and the bond strength of the standard specimen is developed. This relation allows the prediction of the bond strength of the elongated specimen from the bond strength of the standard specimen. The predictive capability is evaluated using data for elongated and standard specimens for selected coatings. The approach is described in the following five steps.

In the first step, two criteria for debonding of the standard and elongated specimens are selected to be evaluated. These criteria are the energy release rate, $\mathcal{G}_I$, and the maximum stress. In the second step, finite-element models of the standard specimen and the elongated specimen are developed, including debonding cracks between the coating and the substrate. A loading to simulate the testing machine force is applied to each finite-element model. In Step 3, the two criteria are evaluated for the standard and elongated specimens for many cases representing a range of values of Young's modulus of the coating, coating thickness, and Poisson's ratio of the thermal spray coating. In Step 4, the results of Step 3 are compared to identify the relation between the bond strengths of the standard specimen and the elongated specimen. In the fifth step, the relation identified in Step 4 is used to predict the bond strength of the elongated specimen using the bond strength of the standard specimen. Comparisons between the predicted debond strengths and experimental data for the elongated specimen are made to evaluate the method for two different coatings and an epoxy.

3. Debonding Criteria

3.1 *Energy Release Rate Criterion*

The energy release rate has been used successfully as a fracture criterion for debonding of epoxy-based composite materials.[7,8] Several authors have used a fracture mechanics approach, based on linear elastic fracture mechanics to characterize the bond strengths of thermal spray coatings. For example, fracture test specimens have been used to produce the Mode I or opening mode of debonding using a double cantilever beam specimen[9] and the Mode II or shear mode of debonding.[10]

The energy release rate, denoted by $\mathcal{G}$, is one of the fracture criteria in linear elastic fracture mechanics and is defined as the energy released per unit area of new crack surface created by crack growth. There are three modes of crack growth: Mode I, the opening mode; Mode II, the shearing mode; and Mode III, the tearing mode. This work focuses on $\mathcal{G}_I$, the energy release rate for Mode I, which for isotropic materials and plane strain conditions, can be expressed as:

$$\mathcal{G}_I = \frac{(K_I)^2}{E(1-\nu^2)} = \frac{\sigma^2(\pi a)}{E(1-\nu^2)} f^2(a, \text{geometry}) \quad [1]$$

where K_I is the stress-intensity factor for Mode I; E is Young's modulus; ν is Poisson's ratio; σ is the average applied stress; a is the crack length; and $f(a, \text{geometry})$ is a function of the crack length and the geometry of the specimen.

Because different materials are involved, the equation for the energy release rate can be written as:

$$\mathcal{G}_I = (K_I)^2 F^2 = \sigma^2(\pi a) F^2 \quad [2]$$

where $F = F(a, \text{geometry}, E_b, \nu_b, E_c, \nu_c)$ and the subscripts b and c denote the base metal and the coating. It is important to note that, because the geometry of the standard specimen is different from that of the elongated specimen, the function $f(a, \text{geometry})$ in Eq 1 for the standard specimen is different from the function for the elongated specimen. The same statement applies to the function $F(a, \text{geometry}, E_b, \nu_b, E_c, \nu_c)$ in Eq 2. Fracture occurs when $\mathcal{G}_I$ reaches a critical value, denoted by $\mathcal{G}_{Icr}$. When debonding occurs, $\mathcal{G}_I$ in Eq 2 becomes $\mathcal{G}_{Icr}$ and:

$$\mathcal{G}_{Icr} = (K_{Icr})^2 F_s^2 = (\sigma_{cr}^s)^2(\pi a) F_s^2 \quad [3]$$

$$\mathcal{G}_{Icr} = (K_{Icr})^2 F_e^2 = (\sigma_{cr}^e)^2(\pi a) F_e^2 \quad [4]$$

where F_s is the function of the geometry and the material properties for the standard specimen, and F_e is the function of the geometry and the material properties for the elongated specimen. The term σ_{cr}^s is the debond stress for the standard specimen, and σ_{cr}^e is the debond stress for the elongated specimen. The critical value of energy release rate, $\mathcal{G}_{Icr}$, is a material property. Therefore, dividing Eq 4 by Eq 3 and taking the square root of the result gives:

$$\frac{\sigma_{cr}^e}{\sigma_{cr}^s} = \frac{F_s}{F_e} \quad [5]$$

or

$$\frac{\sigma_{cr}^e}{\sigma_{cr}^s} = \frac{F_s(a, \text{geometry}, E_b, u_b, E_c, u_c)}{F_e(a, \text{geometry}, E_b, u_b, E_c, u_c)} \quad [6]$$

After F_s and F_e are determined, Eq 6 can be used to find the relation between σ_{cr}^s and σ_{cr}^e. Then, the debond strength of the elongated specimen, σ_{cr}^e, can be predicted from the debond strength of the standard specimen, σ_{cr}^s, from Eq 6.

3.2 *Maximum Stress Criterion*

The axial stress distributions obtained from the finite-element models are shown in Fig. 2. Four characteristics about the stress distributions at the interface can be seen from Fig. 2. First, for both the standard and the elongated specimens, there is a steep stress gradient at the interface near the specimen edge. The second is that the highest stress occurs at the outer radius of the

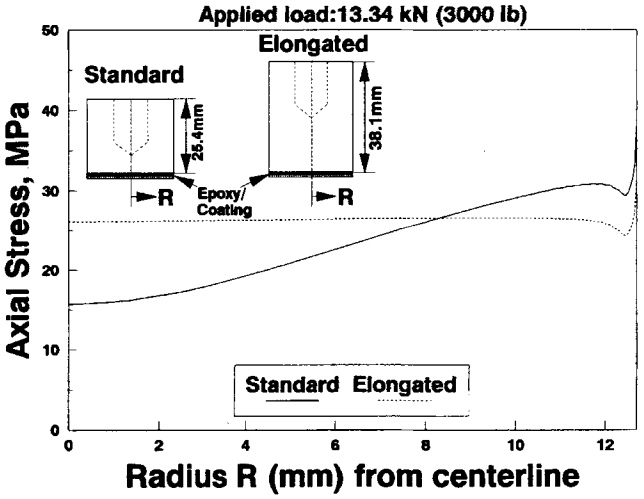

Fig. 2 Axial stress distributions at the coating/base metal interface.

specimen. The third is that the stress distribution for the elongated specimen is more uniform than that for the standard specimen. The last characteristic is that bond stress at the edge (outer radius) is higher for the standard specimen than for the elongated specimen. It is noted that both stress distributions shown in Fig. 2 have an inflection point near the free edge. This is a common free edge effect observed in laminated materials. The effect is the result of the (1) different material properties, E and ν, for the coating, substrate, and epoxy and (2) the requirement to satisfy force and moment equilibrium near the free edge.

Finite-element analysis for the problem with four noded isoparametric elements will provide finite values of the stress. The maximum stress from the finite-element model, however, will have some dependence on the size of the finite elements at the interface near the free edge. Thus, the same size element was used for the finite-element models for the standard and elongated specimens. The ratio of the maximum stresses at the interface between the standard specimen and the elongated specimen can be evaluated. The applied stress and the maximum bond stress can be related as follows:

$$\sigma_B = \sigma_{App} H(\text{geometry, properties}) \quad [7]$$

where σ_B is the maximum bond stress at the interface; H is a function of geometry and material properties of the specimen, and σ_{App} is the average applied stress on the interface. For the standard and elongated specimens,

$$\sigma_B^s = \sigma_{App}^s H_s \quad [8]$$

$$\sigma_B^e = \sigma_{App}^e H_e \quad [9]$$

The ultimate bond stress is σ_{Ult}. When the maximum bond stress at the interface, σ_B, of the standard specimen or the elongated specimen reaches σ_{Ult}, debonding occurs. At debonding,

$$\sigma_{App}^s = \sigma_{cr}^s \text{ and } \sigma_{App}^e = \sigma_{cr}^e \quad [10]$$

Therefore,

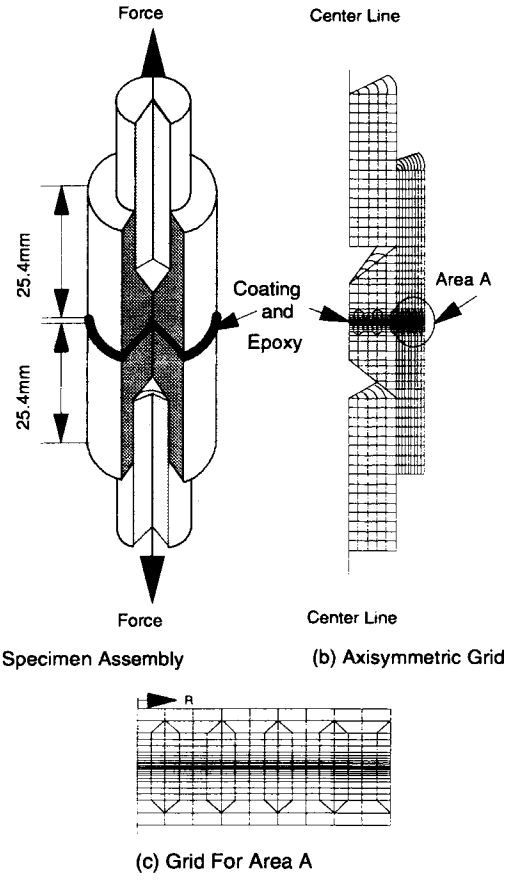

Fig. 3 Finite-element model of C633 standard specimen.

$$\sigma_{Ult} = \sigma_{cr}^s H_s \text{ and } \sigma_{Ult} = \sigma_{cr}^e H_e \quad [11]$$

or

$$\sigma_{cr}^s H_s = \sigma_{cr}^e H_e \quad \sigma_{cr} = \sigma_{cr}^s \frac{H_s}{H_e} \quad [12]$$

After H_s and H_e are determined, Eq 12 can be used to find the relation between the debond stress of the standard specimen, σ_{cr}^s, and the debond stress of the elongated specimen, σ_{cr}^e. Therefore, Eq 12 can be used to predict σ_{cr}^e from knowledge of σ_{cr}^s.

4. Finite-Element Model and Sensitivity Analyses

4.1 *Finite-Element Models*

A finite-element model was developed for both the standard specimen and the elongated specimen to evaluate the energy release rate and maximum stress at the interface between the coating and the substrate. The finite-element model for the elongated specimen is similar to the standard specimen model, except the specimen is longer. Figure 3 shows the standard specimen test configuration and the axisymmetric finite-element model of this

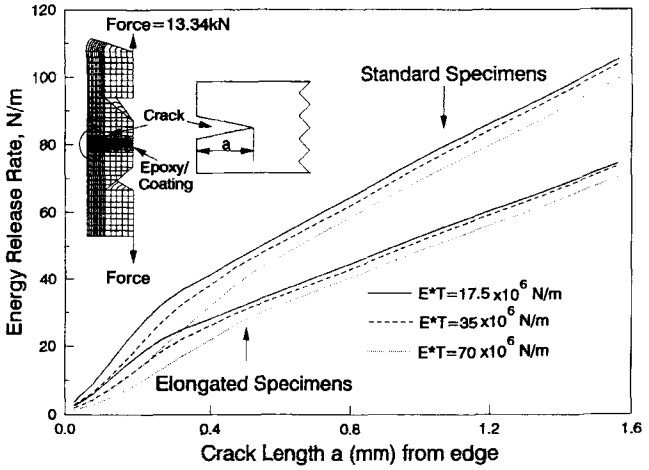

Fig. 4 Energy release rates versus crack length for standard and elongated specimens.

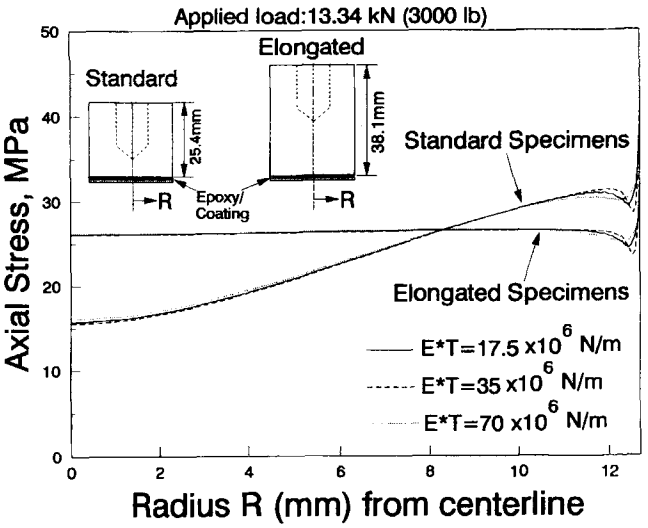

Fig. 5 Axial stress distributions at the coating/substrate interface for different coating properties.

structure. Because the focus of this work is on the interface between the coating and the substrate, the grid is more refined in the regions containing the epoxy, the coating, and the contiguous substrate. The thickness of the finite-element layer nearest the interface is 0.0635 mm (0.0025 in.). A tensile force of 13.34 kN (3000 lb) was applied to the model, as illustrated in Fig. 3.

The finite-element models for both the standard specimen and the elongated specimen have double nodes at the interface between the coating and the substrate. An axisymmetric crack at the interface edge between the coating and substrate was simulated. Crack growth was represented by uncoupling the double nodes to make the crack longer. Energy release rates were evaluated using the modified crack closure integral described in Ref 11. Using a finite-element model of the test specimen containing a crack of length a, the energy to close the crack a small amount, Δa, is calculated. The energy release rate is then evaluated by dividing the energy to close the crack by the area of crack surface closed. Curves of the energy release rate, $\mathcal{G}_I$, versus crack length for the same applied load can be determined for both the standard specimen and the elongated specimen. At a crack length of zero, the maximum stress can be determined from the axial stress distribution across the interface between the coating and the substrate.

4.2 *Sensitivity Analyses*

Sensitivity analyses were conducted to determine the effect of ranges of values of the properties of the coatings on the energy release rate and the maximum stress. The value of Young's modulus and Poisson's ratio for the epoxy used in this study are 3.45×10^3 MPa (0.5×10^6 psi) and 0.34, respectively.[12,13] The coating properties selected for the sensitivity analyses are Young's modulus, Poisson's ratio, and coating thickness. Because coating properties are not generally available, a range of property values was selected. The range of Young's modulus selected was 69×10^3 MPa to 276×10^3 MPa (10×10^6 to 40×10^6 psi). The range of Poisson's ratio was 0.2 to 0.4. The range of coating thicknesses was 0.127 to 0.508 mm (5 to 20 mils). Preliminary studies indicated that the effect of Poisson's ratio of the coating was not very significant. Therefore, the value of Poisson's ratio used in this study was 0.3.

Table 1 Ratio of the energy release rate geometry factors for standard and elongated specimens

	Ratio, N/m (Kips/in.)		
$E \times T$	1.75×10^7 (100)	3.50×10^7 (200)	7.01×10^7 (400)
F_s/F_e	1.209	1.207	1.205

It was also noted that the value of Young's modulus multiplied by the coating thickness can be used as a single parameter for sensitivity analysis. This finding reduced the number of curves required to present all of the sensitivity analysis results (Fig. 4 and 5).

In Fig. 4, the vertical axis shows the energy release rate, and crack length is shown on the horizontal axis. The load was a constant force of 13.34 kN (3000 lb). The upper three lines are for the standard specimen, and the lower three lines are for the elongated specimen. Changes in the slope of the energy release rate values versus crack length curves shown in Fig. 4 at about 0.2 mm are the result of the free edge effect in the stress distribution shown in Fig. 2. As can be seen from Fig. 4, for a fixed crack length and for the same load, the energy release rates for the standard specimen are higher than the energy release rates for the elongated specimen. Because it is assumed that failure occurs when the energy release rate reaches a critical value, this implies that the standard specimen will fail at a lower applied load than the elongated specimen.

Another important finding of these analyses is that the ratio of the energy release rate of the standard specimen to that of the elongated specimen is almost constant for a fixed crack length. Therefore, the ratio of geometry factors for the standard specimen and the elongated specimen can be determined. The results based on the finite-element analyses are shown in Table 1. As shown, for E (Young's modulus) $\times$ T (coating thickness) equal to 1.75×10^7, 3.50×10^7, and 7.01×10^7 N/m (100, 200, and 400 10^3 lb/in.), the ratio of the geometry factor of the standard specimen to the geometry factor of the elongated specimen is about 1.21.

Table 2 Ratio of the maximum stress geometry factors for standard and elongated specimens

	Ratio, N/m (Kips/in.)		
$E \times T$	1.75×10^7 (100)	3.50×10^7 (200)	7.01×10^7 (400)
H_s/H_e	1.219	1.216	1.21

In Fig. 5, the vertical axis is the axial stress at the coating/substrate interface, and the horizontal axis is the radius. The applied load is a force of 13.34 kN (3000 lb) for all cases. The three dotted lines are for standard specimens with different coating properties, and the three solid lines are for elongated specimens with different coating properties. As can be seen in Fig. 5, for the same applied load, the axial stress distributions within a group of specimens (either standard or elongated specimens) are close. However, a large difference exists between the axial stress distributions of the standard specimens and the elongated specimens. This difference implies that the effect of coating properties on axial stress distributions is not very significant. However, the geometry factors cause a difference in axial stress distributions among standard specimens and elongated specimens.

A similar finding of these analyses is that the ratio of the corresponding maximum axial stress between the standard specimen and the elongated specimen is almost independent of coating properties. Therefore, the ratio of geometry factors between the standard specimen and the elongated specimen can be determined. The results based on the finite-element analysis are shown in Table 2. As can be seen, for E (Young's modulus) $\times$ T (coating thickness) equal to 100, 200, and 400 (10^3 lb/in.), the ratio of the geometry factor of the standard specimen to the geometry factor of the elongated specimen is about 1.21.

5. Prediction of Bond Strength for Elongated Specimens

Using the energy release rate as the fracture criterion, from Eq 6, the relation between the bond strength of the standard specimen and the elongated specimen was found to be

$$\sigma_{cr}^{e} = \sigma_{cr}^{s} \frac{F_s}{F_e} \quad [13]$$

Also based on the finite-element analyses:

$$\frac{F_s}{F_e} \cong 1.21 \quad [14]$$

Therefore, using the ratio of the geometry factor of the standard specimen to that of the elongated specimen, the bond strength for the elongated specimen can be predicted from the bond strength data of the standard specimen by the equation:

$$\sigma_{cr}^{e} = 1.21\, \sigma_{cr}^{s} \quad [15]$$

Using the maximum stress as the fracture criterion, Eq 12 gives:

$$\sigma_{cr}^{e} = \sigma_{cr}^{s} \frac{H_s}{H_e} \quad [16]$$

Based on the finite-element analyses:

$$\frac{H_s}{H_e} \cong 1.21 \quad [17]$$

Therefore, using the ratio of the geometry factor of the standard specimen to that of the elongated specimen, the bond strength for an elongated specimen can be predicted from standard specimen data using:

$$\sigma_{cr}^{e} = 1.21\, \sigma_{cr}^{s} \quad [18]$$

Comparing Eq 15 and 18, it can be seen that, using either the energy release rate criterion or the maximum stress criterion, the bond strength of the elongated specimen is predicted to be approximately 1.21 times the bond strength of the standard specimen.

6. Comparing Bond Strength Data and Predictions

6.1 *Bond Strength Data*

Two coatings were selected for testing. One was aluminum oxide, which was applied with the Rokide process. The other was Colmonoy No. 6, which was applied with the Jet Kote II process. The composition of Colmonoy No. 6 is 0.50 to 1.00 wt% C, 12.00 to 18.00 wt% Cr, 2.50 to 4.50 wt% B, 3.50 to 5.50 wt% Si, 3.50 to 5.50 wt% Fe, 0.20 wt% Co max, and 65.00 to 75.00 wt% Ni. For each coating, five standard specimens and five elongated specimens made of 1018 carbon steel were bonded together using a 3M epoxy designated EC-1386. For comparison, five blank standard specimens and five blank elongated specimens were also bonded together using epoxy EC-1386. The procedure delineated in ASTM Standard C 633-79 was followed, and alignment was provided by the double swivel self-aligning fixture shown in Fig. 1. Alignment of the test specimen was found to be uniform around the circumference to within 1.5%.[14] Tensile loads were applied to the specimens using a Materials Testing System (MTS 810), and ultimate loads were recorded. The bond strength (ultimate bond stress) of the epoxy was calculated using the ultimate force divided by the test section cross section area. Bond strengths of the two coatings and the epoxy, as determined by this procedure for both the standard and elongated specimens, are presented in Table 3. The mean values of ultimate bond stresses presented in Table 3 show that the elongated specimens have higher ultimate bond stresses than the standard specimens for the two coatings and epoxy. No intention is made to draw conclusions about variability in the test results.

6.2 *Predicted Elongated Specimen Bond Strengths And Data*

Using either Eq 15 or Eq 18, the predicted debond strengths for the elongated specimen were calculated and are shown in Ta-

Table 3 Ultimate bond stress

Specimen No.	Ultimate bond stress, MPa (psi) Aluminum oxide Standard	Aluminum oxide Elongated	Colmonoy No. 6 Standard	Colmonoy No. 6 Elongated	Epoxy EC-1386 Standard	Epoxy EC-1386 Elongated
1	31.34	(a)	46.42	(a)	56.50	72.81
2	25.55	48.09	40.09	42.54	55.55	74.51
3	27.51	41.95	37.91	41.93	60.77	71.74
4	29.15	44.05	38.78	49.84	55.13	69.63
5	(a)	29.97	38.91	61.47	58.38	72.00
Average	28.39	41.02	40.42	48.95	57.27	72.14
	(4117)	(5949)	(5862)	(7099)	(8306)	(10,463)

(a) Incomplete bonding

Table 4 Average data and predicted bond strengths of elongated specimens

	Prediction MPa	Prediction psi	Test data MPa	Test data psi	Difference, %
Aluminum oxide	34.35	4982	41.02	5949	16.25
Colmonoy No. 6	48.91	7094	48.95	7099	0.07
Epoxy	69.30	10,050	72.14	10,463	3.95

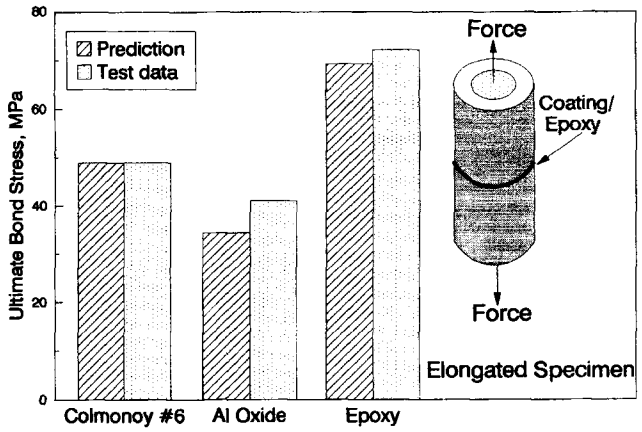

Fig. 6 Comparison of data and predicted ultimate bond stresses for the elongated specimens.

ble 4. Figure 6 shows a graph of the predictions and test data. As shown, for the Colmonoy No. 6 coating, the predicted bond strength agrees with the test data to within 0.1%. For Epoxy EC-1386, the difference between the predicted value and the test data is less than 4%. For the aluminum oxide coating, the difference between the predicted bond strength and the test data is 16.25%.

7. Summary and Conclusions

In previous work, it was shown that the ASTM Standard C633-79 specimen produced stresses along the bonded interface that were not uniform as assumed in the procedure. A more representative specimen for evaluating bond strength was developed. Because a large database exits for the standard specimen, the purpose of the current work is to develop a means to estimate the bond strength that would result from the elongated specimen based on the existing standard specimen data without redoing any tests with the elongated specimens. Using two fracture criteria, finite-element analyses and debond test data showed two interesting and practical results. One result was that both predictions and data indicate that a reasonable estimate of the bond strength can be determined by multiplying the bond strength obtained from the standard specimen by a factor of 1.21. The second result is that, based on the debond criteria and data used in this work, it appears that the factor of 1.21 is independent of coating modulus, thickness, and Poisson's ratio, if both the standard specimen and the elongated specimen have the same material properties, thickness, and are equally well bonded. Thus, it is not necessary to know the modulus, Poisson's ratio, thickness, or defect size of the coating to use the method presented here as long as they are assumed to be the same for both the standard specimen and the elongated specimen.

It should be noted that, although the conclusions presented here agree with the data, there are three assumptions in developing the procedure that should be taken into account when applying the factor of 1.21 to a variety of coatings. One is the assumption that linear elastic fracture mechanics is applicable and that the energy release rate and the maximum stress are valid debonding criteria. Another is that the properties of the standard specimen (modulus, Poisson's ratio, coating thickness, and crack length) are the same for the elongated specimen. The third assumption is that quantities not included in the analysis, such as residual stresses, have the same effect on the standard and elongated specimens. Finally, although the factor of 1.21 appears to be a convenient way to transform the standard specimen data to the elongated specimen data, it is recommended that future debond tests be done with elongated specimens for other coatings.

Acknowledgments

Funding for this research project was provided by The Erosion/Corrosion Research Center at The University of Tulsa and

The Oklahoma Center for the Advancement of Science and Technology (OCAST).

References

1. W. Han, E. F. Rybicki, and J. R. Shadley, Bond Strength Testing of Thermal Spray Coatings Using ASTM C633-79—Effect of Specimen Size on Test Results, *Thermal Spray: International Advances in Coating Technology*, C.C. Berndt, Ed., ASM International, 1992, p 911-914
2. ASTM Designation C 633-79, Standard Test Method for Adhesion or Cohesive Strength of Flame-Sprayed Coatings, *The Annual Book of ASTM Standards*, American Society for Testing and Materials, 1982
3. R.H. Unger and W.D. Grossklaus, A Comparison of the Technical Properties of Arc Sprayed Versus Plasma Sprayed Nickel-5 Aluminum, *SAE Technical Paper Series*, 28th Annual Aerospace/Airline Plating & Metal Finishing Forum & Exposition, San Diego, 1992
4. P. Ostojic and C.C. Berndt, The Variability in Strength of Thermal Sprayed Coatings, *Surf. Coat. Technol.*, Vol 34, 1988, p 43-50
5. S.D. Brown, B.A. Chapman, and G.P. Wirtz, Fracture Kinetics and Mechanical Measurement of Adherence, *Thermal Spray Technology*, D.L. Houck, Ed., ASM International, 1989, p 147-157
6. Y. Shimizu, M. Sato, K. Maeda, and M. Kabayashi, Effect of Test Specimen Size upon Adhesive Strength of Flame Sprayed Coatings, *Thermal Spray Coatings: Properties, Processes and Applications*, T.F. Bernecki, Ed., ASM International, 1991, p 257-262
7. E.F. Rybicki, D.W. Schmueser, and T. Fox, An Energy Release Rate Approach for Stable Crack Growth in The Free-Edge Delamination Problem, *J. Composite Mater.*, Vol 11, Oct 1977, p 470-487
8. E.F. Rybicki, T.D. Hernandez, Jr., J.E. Deibler, R.C. Knight, and S.S. Vinson, Mode I and Mixed Mode Energy Release Rate Values for Delamination of Graphite/Epoxy Test Specimens, *J. Composite Mater.*, Vol 21, Feb 1987, p 105-123
9. C.C. Berndt, "The Adhesion of Flame and Plasma Sprayed Coatings," Ph.D dissertation, Dept. of Materials Engineering, Monash University, Victoria, Australia, 1980
10. P.J. Callus and C.C. Berndt, A Shear Test for Thermal Sprayed Coatings, *Proc. 12th Int. Conf. Thermal Spraying*, London, 1989
11. E.F. Rybicki, and M.F. Kanninen, A Finite Element Calculation of Stress Intensity Factors by A Modified Crack Closure Integral, *Eng. Fract. Mechan.*, Vol 9, 1977, p 931-938
12. H. Lee and K. Neville, *Handbook of Epoxy Resin*, McGraw-Hill, 1967
13. G.F. Kinny, *Engineering Properties and Applications of Plastics*, John Wiley & Sons, 1964
14. W. Han, E.F. Rybicki, and J.R. Shadley, An Improved Specimen Geometry for ASTM C633-79 to Estimate Bond Strengths of Thermal Spray Coatings, *J. Thermal Spray Technology*, Vol 2 (No. 2), June 1993